The Impact of Crop Areas in Northeast Colorado on Midsummer Mesoscale Thermal Circulations

M. SEGAL,* W. E. SCHREIBER,[†] G. KALLOS,[‡] J. R. GARRATT,[*,§] A. RODI,[†]
J. WEAVER[*,@] AND R. A. PIELKE*

*Department of Atmospheric Science, Colorado State University, Fort Collins, Colorado
[†]Department of Atmospheric Science, University of Wyoming, Laramie, Wyoming
[‡]Department of Applied Physics, University of Athens, Greece
[@]NOAA/NESDIS/RAMM Branch

ABSTRACT

The present study provides a preliminary evaluation of mesoscale circulations forced by surface gradients of heating arising from irrigated areas adjacent to dry land, utilizing a combination of satellite, observational, and modeling approaches. The irrigated crop areas of northeast Colorado were chosen for the study. For the cases studied satellite surface infrared temperature data indicated a typical temperature contrast of approximately 10 K at noon, between the irrigated area and the adjacent dry land. Surface observations and aircraft measurements within the lower region of the atmospheric boundary layer indicated, in general, a significant temperature contrast and moisture difference, thereby implying a potential thermally driven circulation. The anticipated thermally induced flows, however, were reflected in the measurements only by modest changes in the wind speed and wind direction across the contrast location. It is suggested that the daytime, elevated, terrain-forced flow in the area, and the synoptic flow, combined to mask to varying degrees the thermally induced circulation due to the irrigated land–dry land area effect. Numerical model simulations which were carried out over the studied area support this hypothesis. In addition, the impact of the irrigated areas on the moisture within the boundary layer, as well as on potential convective cloud development, is discussed.

1. Introduction

Summer irrigated crop areas generally have a significantly lower Bowen ratio (the ratio of surface sensible heat flux, H_s, to that of evapotranspiration flux, H_L) when compared to dry land areas. Since the available net radiation at the surface, less the soil heat fluxes, is partitioned between H_s and H_L at the surface, it follows that the presence of a large irrigated area adjacent to a dry area, within a mesoscale domain, should result in substantial horizontal gradients in H_s. Consequently, a horizontal temperature gradient within the lower atmosphere, analogous to that found along a seacoast, should result, and a sea-breeze-like circulation [termed in this paper a *nonclassical mesoscale circulation* (NCMC) to distinguish it from the sea breeze which is also forced by horizontal gradients in H_s] is expected to be induced. Theoretical and conceptual evaluations of the kinematic and thermodynamic processes asso-

ciated with NCMC in such situations have been provided in recent years, for example, by Smith and Mahrt (1981), Anthes (1984), Segal et al. (1984), and Pielke and Segal (1986). Numerical model studies by Mahfouf et al. (1987) and Segal et al. (1988) suggested that for dense, well-watered and *extended* crop areas, mesoscale circulations of an intensity close to that of a sea breeze may be produced. In Segal et al. (1988), a short review of previous studies relevant to NCMCs was included. Also worth noting are observational studies in the early fifties in the semiarid Trans Volga steppe in the Soviet Union (although they involved relatively coarse resolution measurements), which suggested the existence of NCMCs involved with irrigated areas (Dzerdzeevskii 1963). It has been suggested that NCMCs along irrigated wet land–dry land contrasts may be of some significance in convective cloud initiation under supportive synoptic conditions (Sun and Ogura 1979; Anthes 1984; Yan and Anthes 1988). Likewise, cloud-scale model simulations by Smolarkiewicz and Clark (1985) suggested that inhomogeneities in soil and vegetation characteristics are likely to be important in the early stages of cumulus cloud formation.

Since in the aforementioned model simulation studies, prescribed vegetation characteristics were used, observational studies should next be carried out in order to evaluate thoroughly whether real-world, large

---

§ Permanent affiliation: CSIRO, Division of Atmospheric Research, Mordialloc, Victoria, Australia.

Corresponding author address: Motie Segal, Colorado State University, Dept. of Atmospheric Science, Fort Collins, CO 80523.

irrigated areas, might produce significant NCMC development. The need for observations mostly emerges due to the complexities involved with defining the characteristics of real world, irrigated areas (e.g., area boundaries, crop areal density, crop type, evapotranspiration as affected by the environmental conditions, etc.) in numerical models. In order to perform a preliminary case-study evaluation in the United States, aircraft measurements were made in northeast Colorado during the CINDE (Convective Initiation and Downburst Experiment) project in the summer of 1987. In addition, comprehensive GOES (Geostationary Operational Environmental Satellite) imagery was collected throughout the summer of 1986 over corresponding areas, in order to determine typical infrared (IR) surface temperature fields in that location. The PROFS (Program for Regional Observing and Forecasting Systems) network data were also available for these evaluations.

The present study describes observational analyses performed using these data. The study also involves several numerical model simulations for the area, in order to provide further general insight into the impact of the chosen irrigated areas on mesoscale processes. In addition, evaluation of the impact of the involved irrigated areas on several planetary boundary-layer (PBL) properties is included.

2. Description of the experimental area

The irrigated areas which were chosen for the present study (see Fig. 1) consist of portions of the Front Range of Colorado, mostly in the region between the cities of Fort Collins, Longmont, and Greeley. During the summer, this area (indicated by dots in Fig. 1) is densely
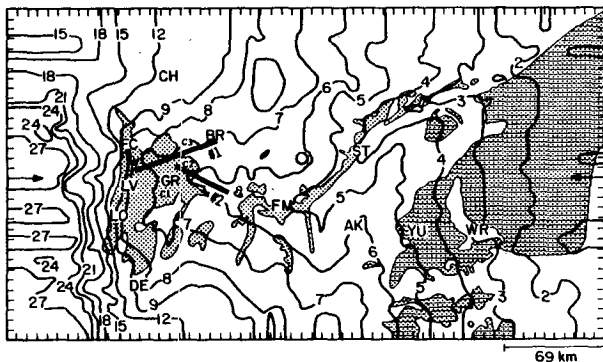

FIG. 1. Map indicating the irrigated areas and illustrating the topography of the study area (described in text). The irrigated areas along the South Platte River are indicated by dots; the semiirrigated areas are indicated by shaded dots (reproduced from map of *Important Farmlands of Colorado*, prepared by USDA-Soil Conservation Service and CSU Experiment Station, Fort Collins, Special Series 17, 1980). The terrain heights are given in hundreds of meters relative to the lowest elevation in the domain (820 m AMSL). The illustrated domain was used in the simulations described in section 5. The thick lines No. 1 and No. 2 indicate the flight transects.

covered by irrigated crops (~70%) including corn, beans, alfalfa, and sugar beets. In addition the semiirrigated Yuma-Wray area (indicated by shaded dots in Fig. 1) toward the eastern border of Colorado (which extends into Kansas and Nebraska) is also considered in the study. About 20%–40% of this area is irrigated in July where the major crops are corn and beans. By July, the region surrounding the irrigated areas is typically dry, and thus, in general, sharp contrasts in moisture and temperature between the irrigated area and the dry land are anticipated. The terrain in this region (illustrated in Fig. 1) consists of the South Platte River basin and the Rocky Mountains to the west, leading to the development of significant daytime thermally induced upslope flow over the whole area (e.g., Toth and Johnson 1985). Such flow is likely to affect the irrigated areas, even though the terrain variations in these areas are relatively small.

3. Satellite surface IR imagery

Horizontal variations in surface temperature observed by satellite should provide a preliminary indication of possible induced NCMCs. In order to identify such regions in the experimental areas, a GOES IR black body surface temperature composite of the last 2 weeks in July 1986 was compiled. These data were also used in the present study to initialize and to thermally force a numerical mesoscale model to simulate possible NCMCs in the area, as reported in section 5.

a. Data and data processing systems

Satellite data processing was done through the Interactive Research and Imaging System (IRIS) managed by Colorado State University (CSU). The main processor on the system is a VAX 11/780, and image manipulation is carried out on a two-station, COMTAL Vision One/20 system. Among other available features, the system allows an operator to view imagery for quality control, "roam" imagery on the screen to ensure accurate navigation, and to alter picture element (pixel) brightnesses as required. For a more complete description of the CSU system, refer to Green and Kruidenier (1982).

b. Data analysis techniques

Satellite data used in this study were the 4 × 8 km pixel resolution, thermal infrared wavelength imagery (IR) collected from the GOES. These images are routinely available from GOES every 30 min, but in this study, only hourly data were processed. The data were collected and processed at the CSU direct readout satellite ground station. Before beginning data analysis, the operator first renavigates all of the images to eliminate geographical mismatches due to satellite wobble, navigation parameter errors, etc. This is accomplished

using a fiducial image, and various features of the COMTAL interactive processor.

Once all of the images are matched, the digital counts at each location can be computer averaged. The averages for this study were based upon a scheme in which cloudy areas on each picture are turned pure black, and noncloudy IR pixels left alone. When this new image set is produced, images may be constructed which represented an average skin temperature at each location on the picture. Note that in this scheme, different pixels might have a different number of days in the average, due to variations in cloudiness. However, no pixel is allowed to have less than 4 days in the average. Such pixels, as well as pixels that are always cloudy, are left pure black.

c. IR surface temperature estimates

Selective composites of IR blackbody surface temperature derived from the GOES for 1000, 1100, 1300, and 1400 MDT (mountain daylight savings time = UTC − 6 h) are presented in Fig. 2 and provide insight into the daily surface warming. The irrigated areas indicated in Fig. 1 correspond to the areas of reduced blackbody surface temperature evident mostly at noon hours in Fig. 2. A contrast of about 10 K is evident by 1400 UTC (Fig. 2d) over the Greeley–Briggsdale area along the flight transect No. 1 indicated in Fig. 1. A somewhat smaller contrast is observed across the Yuma–Wray irrigated area eastward. It can

be assumed that the actual IR surface temperatures are somewhat higher than the satellite derived blackbody values for two reasons: first, a small amount of the radiation observed by the satellite instrument originates in the atmosphere, which is cooler than the surface for the studied cases; second, the emittance of the earth's surface is less than 1. On the other hand, the emittance of the irrigated area is likely to be somewhat higher than that of the surrounding dry land (e.g., Lee 1978). Therefore, the actual surface temperature gradients would probably be somewhat larger than those presented. As suggested, for example, in Segal et al. (1988), a surface temperature contrast of this magnitude is likely to produce a noticeable thermal circulation in the absence of background flows and when extended crop areas are involved. It should also be emphasized that (i) because of the averaging involved with the composites, smaller temperature contrasts result as compared to what are found on individual days under clear sky conditions. However, the composite generally provides better information concerning the *typical* areas affected by irrigation; (ii) Since the satellite image has a pixel resolution of 4 km × 8 km some smoothing of the actual temperature contrasts must result.

4. Aircraft, PROFS, and radiosonde observations

The NCAR King Air research aircraft flew transects of the experimental area, measuring the thermodynamic and kinematic properties over the dry and ir-
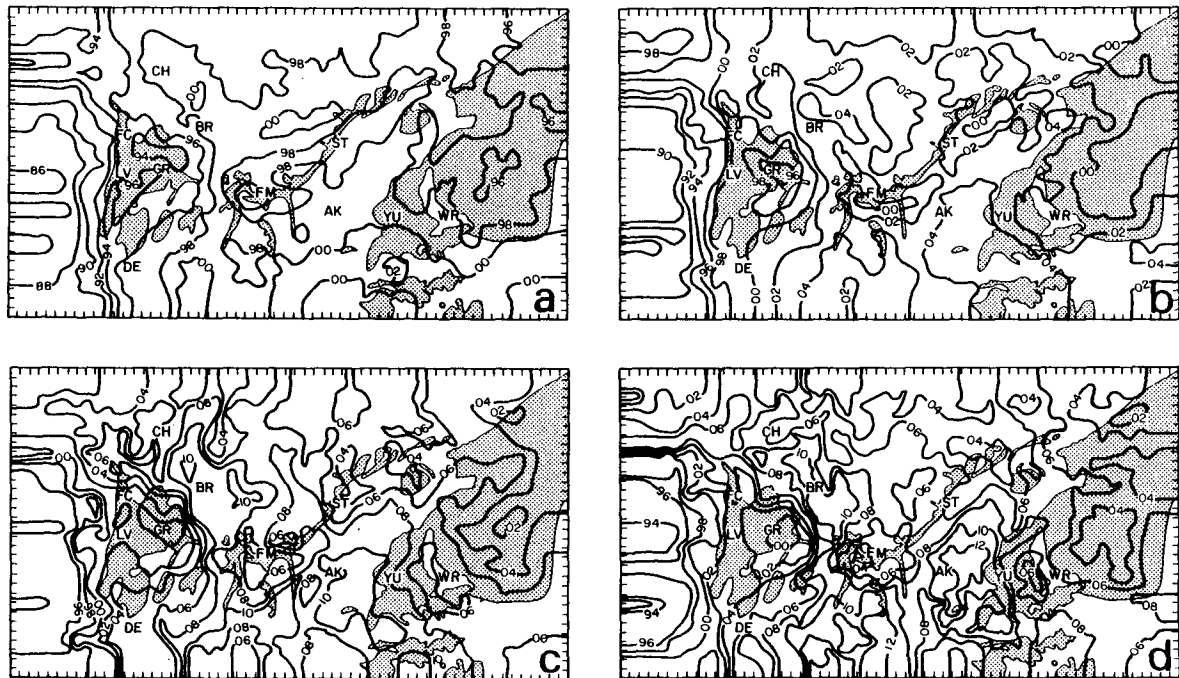

FIG. 2. Composite of GOES-derived IR surface temperature (in K; only the last two digits of the temperature values are indicated on the contours) under clear sky conditions (see section 3) over northeast Colorado for the period 16 July–30 July 1986 for the hours (a) 1000, (b) 1100, (c) 1300, and (d) 1400 MDT. Contour interval 2°K; the irrigated areas are indicated by shading.

rigated areas at varying distances above the ground. Winds were derived from ground velocity measurements from the inertial navigation system (INS) and relative air velocity measurements from the differential pressure probe using the radome technique (Brown et al. 1983). Moisture variables were derived from dewpoint temperature measured by the EG&G model 137 thermoelectric hygrometer. Wind, temperature, and moisture measurements were made on all the flights.

An Epply pyrgeometer, mounted on the bottom of the aircraft and sensitive to surface longwave radiation in the range 3.5–50 μm, was available on the flight of 16 July 1987 only. The flux data shown here were corrected for errors caused by the varying pyrgeometer dome and sink temperatures.

Data were recorded on the aircraft at 50 samples sec^{-1} after being filtered with low-pass filters at 10 Hz cutoff as described by Miller and Friesen (1985). The data shown in this paper are 1 sec (100 m) averages of the 20 samples sec^{-1} archived data.

Three flights were conducted in cooperation with the CINDE project: 16, 25, and 28 July (denoted in the present paper as flights 16, 25, and 28, respectively). The flights were carried out along the two transects, Nos. 1 and 2, depicted in Fig. 1. Flight 16 involved a single circuit at a height of 180 m above ground, while flights 25 and 28 consisted of four legs at the approximate heights of 160, 250, 350, and 445, and 140, 240, 345, and 440 m, respectively. Fluctuations in the flight level above the local terrain (standard deviation of ±20 m) occur mainly due to the influence of convective thermals. Careful examination of horizontal variations of atmospheric properties (along any one flight level) and variations in aircraft altitude revealed no significant correlation between the two. Therefore, within the context of the present study, any significant variations in temperature, moisture, or wind along each flight level are related predominantly to forcing by the underlying surface.

The observational analyses of the PBL thermal contrasts between the irrigated area section of the transects and the dry land section are given and discussed below. The flights were carried out around noon; therefore, flow features should be affected considerably by the daytime thermally induced upslope flows (e.g., Toth and Johnson 1985). In addition to the flight observations, selected surface observations for three sites (Loveland, Greeley, and Briggsdale), as well as radiosonde profiles within the flight area, are presented. A map illustration of the area involved with the observations is given in Fig. 1.

a. Flight 16

This flight was associated with clear sky conditions in the transect area, although the surrounding area was partially covered with convective clouds. The synoptic flow was light and southerly, with the thermally in-

duced upslope flow over elevated terrain turning the winds to a southeasterly direction. The PROFS mesonet surface observations during the flight (Fig. 3) indicate comparable air temperatures at Briggsdale (which is located in the dry land area), and Loveland and Greeley (which are located in the irrigated area). However, noticeably lower dew point temperatures were measured at Briggsdale with wind speeds there larger than those at the other two stations, and winds consistently from the south.

1) TRANSECT NO. 1 (1129–1138 MDT)

The upward surface IR fluxes from the pyrgeometer measurements (Fig. 4a) reflect the general differences in surface characteristics along the flight transect. These fluxes imply black body surface temperatures as low as 300 K over the irrigated area, and as high as 318 K over the dry land. Fluctuations in the IR fluxes are most likely due to aircraft passage over regions of alternating land use, as evaluated from the flight videocassette recorder. However, differences in crop growth stage, land cultivation, and crop cover also contribute to some of the fluctuations.

Variations in the potential temperature, θ (Fig. 4b) correlate, in general, to the IR fluxes depicted in Fig. 4a. The change in θ between the irrigated area (a minimum value of approximately 313 K) to the dry area (maximum value of approximately 316 K) within the context of a NCMC is significant.
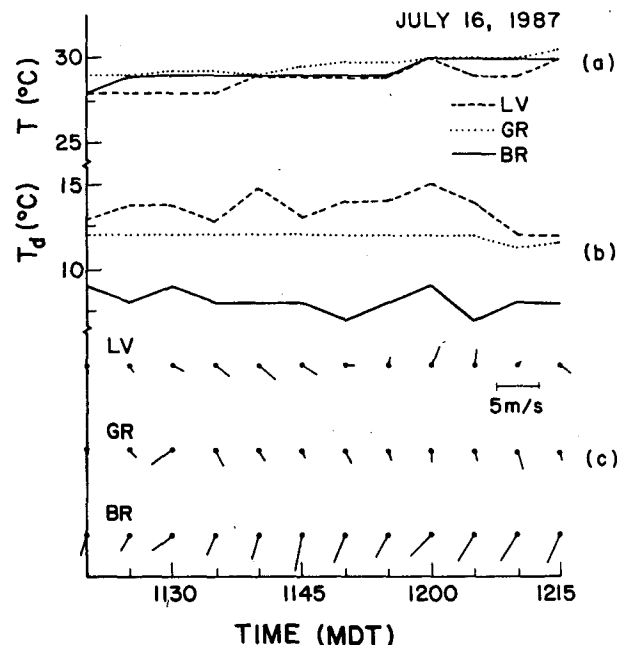

FIG. 3. The PROFS mesonet surface observations at Loveland (LV), Greeley (GR), and Briggsdale (BR) during flight 16: (a) air temperature, (b) air dew point temperature, and (c) wind velocity (flow direction is toward the dot marks).
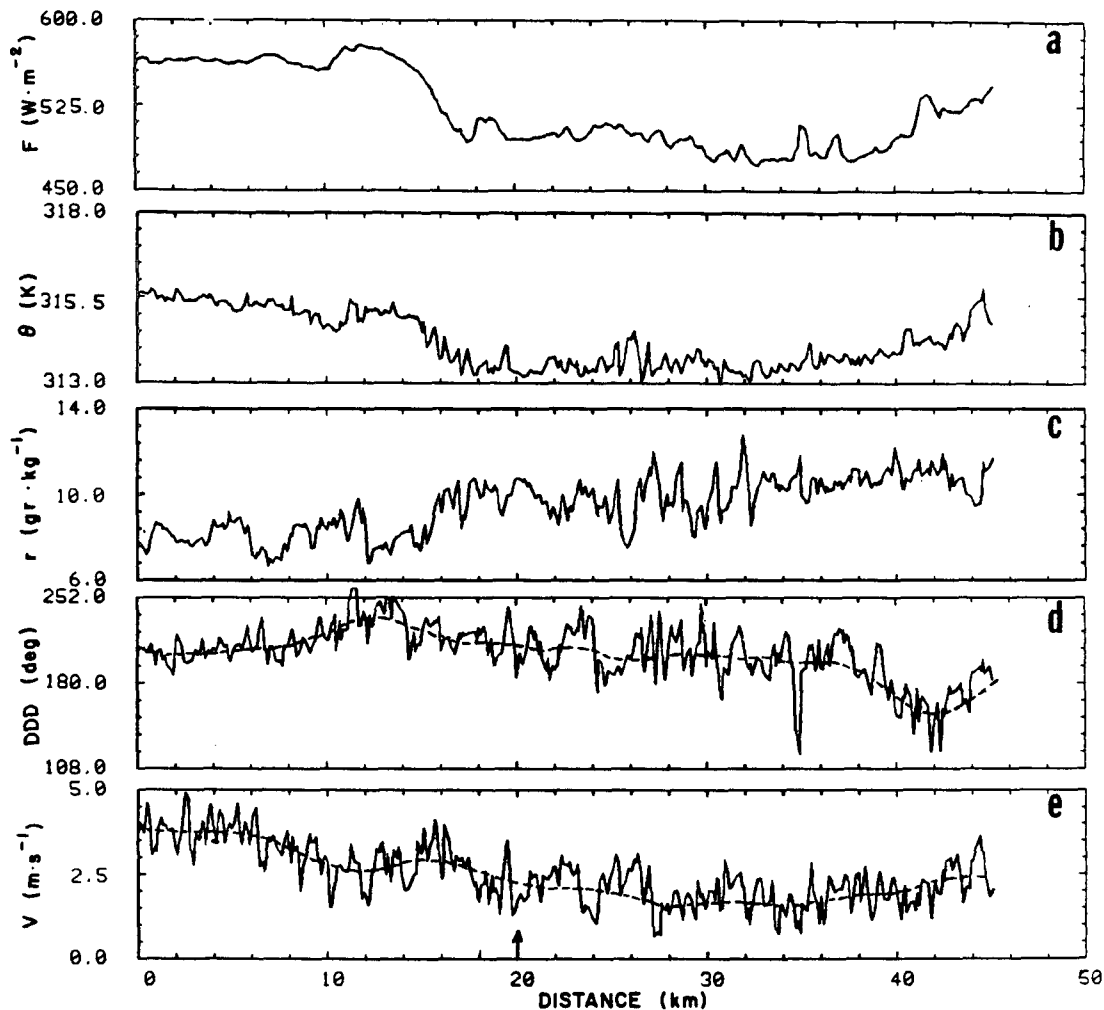
FIG. 4. Measured meteorological variables for flight 16 along transect No. 1 from Briggsdale (dry land) to Windsor (irrigated area) (Briggsdale and Windsor are indicated respectively by BR and W in Fig. 1) at the altitude of ≈180 m above ground level: (a) surface IR radiative flux, (b) potential temperature, (c) moisture mixing ratio, (d) wind direction, (e) wind speed [in (d) and (e) the dashed lines indicate a subjective estimate of the running mean]. The location of the observed crop-dry land boundary is indicated by an arrow.

Note that, while the PROFS temperature trace at Loveland is generally somewhat cooler than that at Briggsdale (as one would expect from the satellite and aircraft observations), the temperature trace from Greeley does not indicate this contrast (Fig. 3). Furthermore, the measured difference between the Loveland and Briggsdale sites is less than that observed by aircraft (i.e., about 1.5 K as opposed to 3 K). It is not known why the thermal contrast is not as large in the surface measurements, but possible reasons include the fact that the PROFS instruments are sited quite differently. Briggsdale is located on dry plains; the Greeley station is at the Weld County airport; and the Loveland station is situated to the east of town on highway 34, adjacent to mixed rural/suburban land usage on nearly flat terrain; i.e., urban effects may modify the surface temperature differences between these sites.

Another factor affecting the surface observations in this case might be the moderate winds over the region. Such flow could be expected to enhance locally near-surface mixing. In fact, when the flow is light and variable (as in the case of Flight 28, discussed later), the PROFS temperature contrast is more pronounced.

Very pronounced variations are evident in the mixing ratio (Fig. 4c), with maximum specific humidity variations at this altitude reaching around 6 g kg^{-1} along the transect between the nonirrigated prairie grass and the irrigated land. The variations are due to increased evapotranspiration over the irrigated land as compared to reduced evapotranspiration over the dry land and the suppression of the PBL depth over this area as compared to that over to the dry land (see Fig. 16a for a comparison of the PBL over the irrigated land as contrasted with the dry land region). Such

suppression, which is evident in the simulations presented in Segal et al. (1988), is related mainly to a reduction in the sensible heat fluxes over the irrigated areas. Subsidence involved with the thermally induced upslope circulations as well as a possible NCMC would contribute furthermore to the suppression of the PBL.

Wind variations along the transect imply average changes in the wind direction of about 60 deg (from about SW over the dry land to about S-SE over the irrigated area), and in the wind speed of about 2.5 m s^{-1} (Figs. 4d,e). The changes in the wind direction and the magnitude of the horizontal temperature gradient suggest the establishment of NCMC flow effects (see scaling evaluations in subsection 4d). As stated previously, coupling of the upslope flow and the prevailing synoptic flow will tend to distort, to various degrees, any NCMC. The existence of NCMC flows as suggested in the current case are evident mainly in variations of the wind velocity, although such variations may also be attributed to the impact on the PBL by the change in surface roughness and wetness between the dry land and the irrigated area. In order to evaluate this aspect, numerical model sensitivity simulations were performed (with a two-dimensional (2-D) version of the model described in section 5) involving a prescribed change in surface roughness and wetness analogous to that associated with the studied area (in which, however, the mesoscale horizontal pressure gradient contribution to the flow acceleration was suppressed). The results indicated that the impact of the change in the surface roughness on the flow should be almost unnoticeable at the flight level.

2) TRANSECT NO. 2 (1154–1200 MDT)

Transect No. 2 of flight 16 lies along a northwest–southeast line near the South Platte River. Features similar to those observed in transect No. 1 were also obtained in the present transect. The IR blackbody surface temperature derived from the upward long wave fluxes (Fig. 5a) yields a large surface temperature contrast of about 15 K. A potential temperature change at the flight level of about 5 K is observed across a distance of about 25 km (Fig. 5b), with the decrease in the mixing ratio over the dry land being more significant than in the previous transect (Fig. 5c). A small variation in wind speed of about 1 m s^{-1} and a change of about 100 deg in wind direction along the transect were observed (Fig. 5d, e).

b. Flight 25 (1413–1458 MDT; transect No. 1)

This flight was carried out under clear sky conditions; however, a synoptic scale pressure gradient interacting with a well-developed daytime upslope flow resulted in a background low-level flow of about 7 m s^{-1} from the dry land to the irrigated region. With this intensity of background flow, and the above normal lower atmospheric air temperatures, the low-level thermal structure over the irrigated area will be strongly affected by the warm air advection. The situation is analogous to that at a coastline, where an offshore synoptic flow is known to be a major factor in determining the height and intensity of shallow surface inversions (or internal boundary layer) immediately offshore (e.g., Mahrer and Segal 1979; Garratt 1987; Garratt and Ryan 1988).
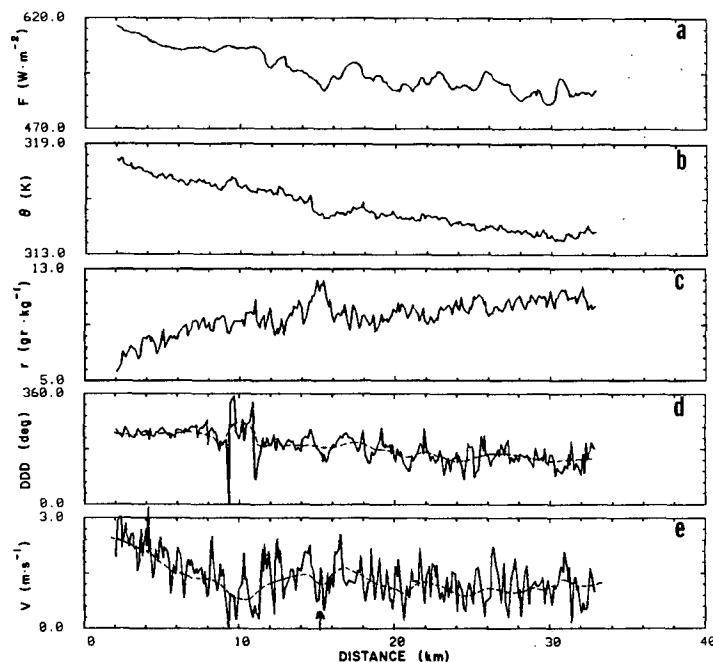

FIG. 5. As in Fig. 4 except for transect No. 2 (beginning is in the dry land area).

In addition, warm air advection is likely to produce a reduction in transpiration from the crops, below the potential rate found under normal summer day weather conditions, due to partial stomatal closure (e.g., Jarvis and Morison 1981). Consequently, an additional reduction in the θ contrast may result, combined with that caused by the warm air advection.

The PROFS stations (Fig. 6) indicate a small surface–air temperature difference between Greeley and Briggsdale which, in part, may be attributed to the westward warm advection in addition to the effects discussed previously for flight 16. Loveland's air temperature, however, is noticeably lower than that of Briggsdale, while the dew point temperature at Loveland (irrigated area) is appreciably higher than Briggsdale (dry land). The stations at Greeley and Loveland show lower wind speed which may be attributed, in part, to the impact of the thermally induced flow interaction with the background flow. However, it should be pointed out that the location of the Greeley and Loveland stations in the lower portion of the south
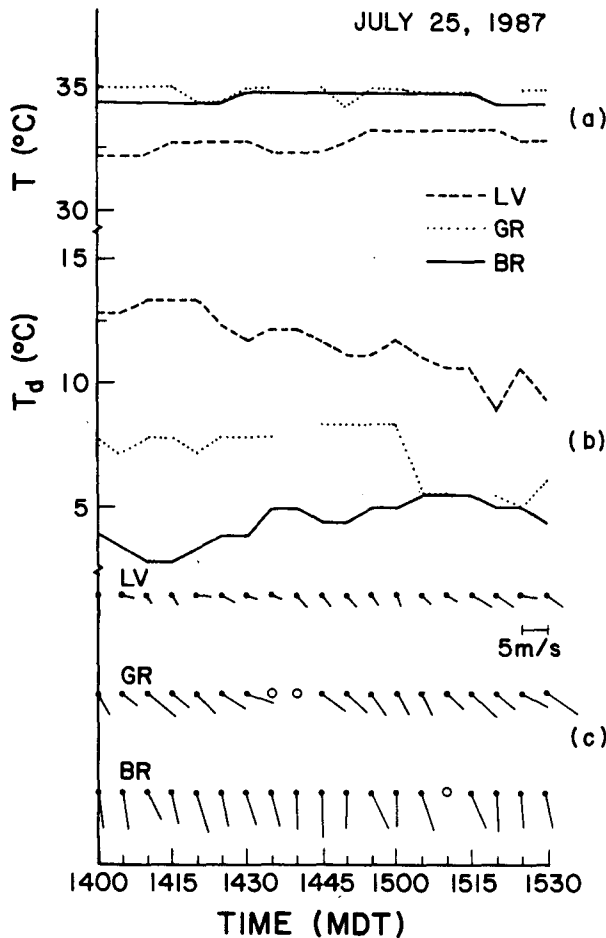

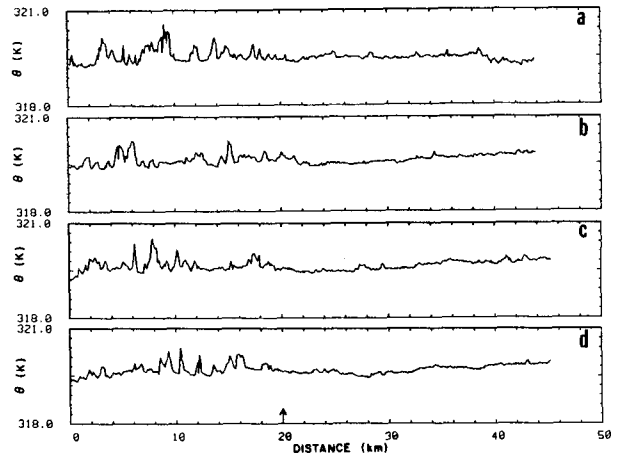FIG. 7. Measured potential temperature for flight 25 along transect No. 1 from Briggsdale to Windsor at the altitudes of (a) ≈160 m, (b) ≈250 m, (c) ≈350 m, and (d) ≈445 m, above the ground level. The location of the observed crop-dry land boundary is indicated by an arrow.

FIG. 6. As in Fig. 3 except for flight 25 (open circles indicate missing data).

Platte river basin should cause some reduction of daytime upslope flow there due to flow divergence, as evident, for example, in Abbs and Pielke (1986).

Figure 7 presents the potential temperature along the transect at various altitudes, where contrasts are noticeable at ±10 km from the location of the crop-dry land boundary. At the height of 160 m, the contrast in θ is mild and significantly smaller than that obtained in flight 16, although it is evident that the potential temperature contrast closely maintains its magnitude for all the elevated transects. Over the irrigated area, the fluctuations in θ are noticeably weaker than in flight 16, suggesting an additional stabilization of the lower atmosphere as the warm air is advected over the relatively cooler crop canopies. This feature of turbulence suppression over the irrigated area is also very pronounced in the elevated legs.

The mixing ratio values at 160 m show a substantial variation along the transect (Fig. 8) although somewhat smaller as compared to values from flight 16. The variation reduces with increased altitude although a significant horizontal atmospheric moisture contrast still exists at 445 m. It is worth noting that fluctuations of the mixing ratio over the irrigated area are significantly larger than those of θ. This feature is attributed to the intense surface moisture source of the irrigated segment and its own irregularities, where the surface heat fluxes should be suppressed. These features are reversed over the dry land where the surface heat fluxes are likely to be intense, but the surface moisture flux is very low.

The wind direction (Fig. 9) and wind speed (Fig. 10) traces indicate variations between the irrigated areas and the dry land; larger wind speeds being measured over the dry land (wind directions typically south easterly) as compared to irrigated areas (with a typical
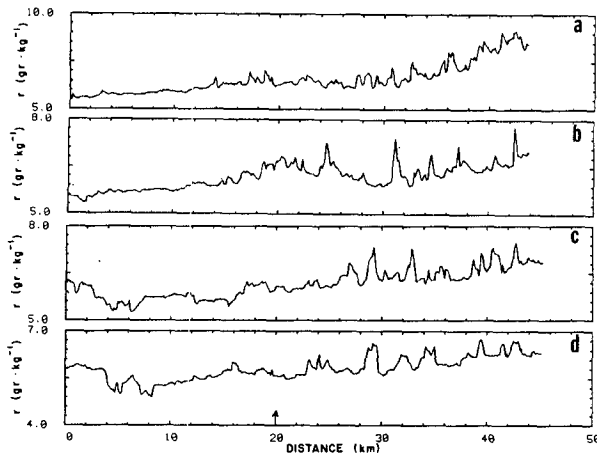
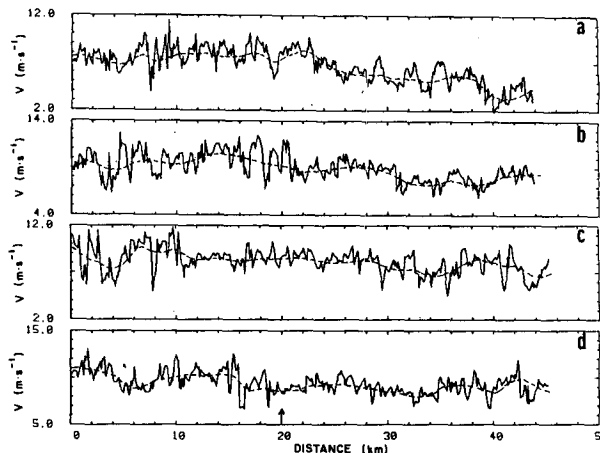FIG. 8. As in Fig. 7, except for moisture mixing ratio.

FIG. 10. As in Fig. 7, except for wind speed (the dashed line indicates a subjective estimate of the running mean).

wind direction from the east). This may suggest coupling of a weak NCMC flow with the relatively strong background flow.

c. Flight 28 (1211–1257 MDT; transect No. 1)

Flight 28 was carried out under clear sky conditions with a light northeasterly synoptic flow; it followed a pronounced dry period and was thus potentially ideal for the identification of NCMCs.

The PROFS stations show significant temperature differences corresponding to the land use along the transect, while the dew point temperatures do not reflect a similar contrast (Figs. 11a and b). The surface wind speed shows a mild general trend of weaker winds in Loveland and the strongest winds in Briggsdale. In general, the wind direction (Fig. 11c) is variable, showing a tendency towards easterly flow. Note that

the wind direction at Loveland before 1230 MDT may imply a thermally induced flow opposing the general flow.

The potential temperature difference between dry and irrigated areas for flight 28 at 140 m is lower than in flight 16, reaching only 2 K, and reduces to approximately 1.5 K at 440 m (Fig. 12). The moisture mixing
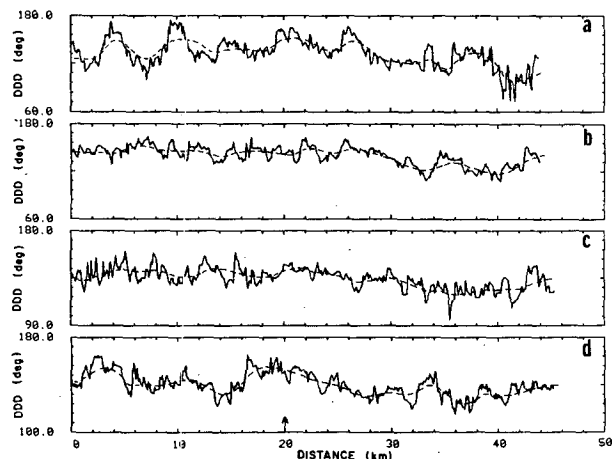

FIG. 9. As in Fig. 7, except for wind direction (the dashed line indicates a subjective estimate of the running mean).
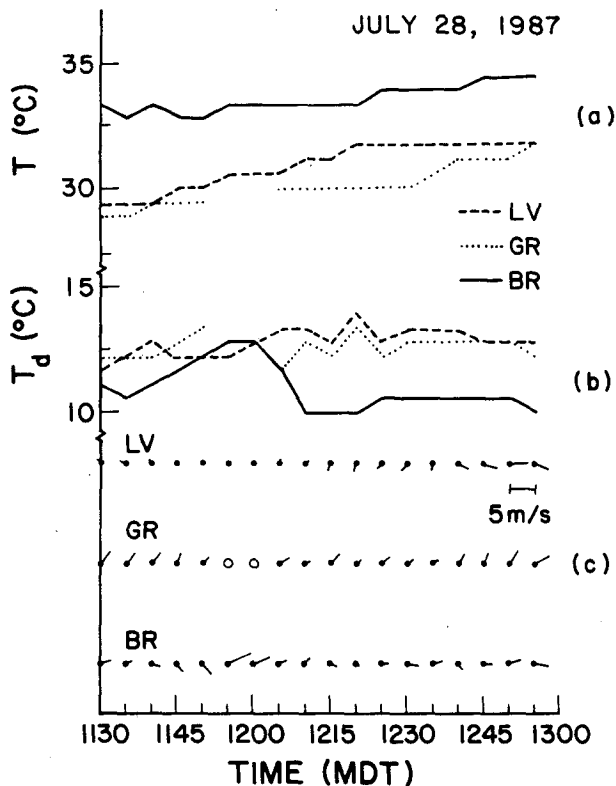

FIG. 11. As in Fig. 3, except for flight 28 (open circles indicate missing data).
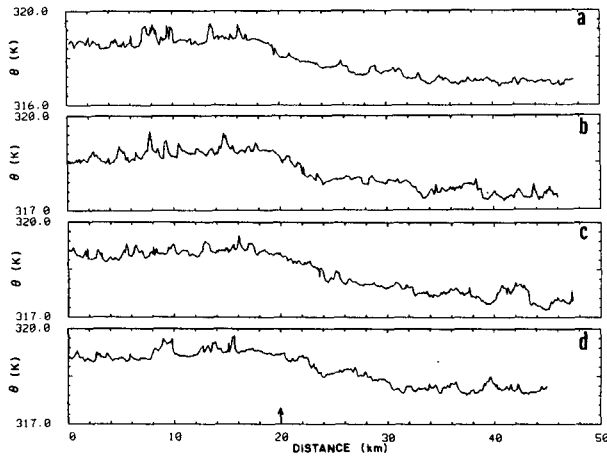
FIG. 12. Measured potential temperature for flight 28 along transect No. 1 from Briggsdale to Windsor at the altitude of (a) ≈140 m, (b) ≈240 m, (c) ≈345 m, and (d) ≈440 m above the ground. The observed crop-dry land boundary is indicated by an arrow.

FIG. 14. As in Fig. 12, except for wind direction and wind speed (the dashed line indicates a subjective estimate of the running mean).

ratio variation along the transect is significant at all altitudes (Fig. 13). Wind direction and speed changes along the various legs between the irrigated area and the dry land are given in Figs. 14 and 15; they generally indicate that over the irrigated area, turbulence levels are lower than over the dry land area (similar to flight 25). However, when subjectively averaging out the turbulence fluctuations, a noticeable change in the wind direction and speed in the legs along the boundary of the irrigated area–dry land line is evident. These changes are attributed to NCMC coupling with the opposing prevailing NE background flow. At the 140 m leg (Figs. 14a, 15a), this coupling is established around the irrigated–dryland boundary, inducing a SE-S flow with a pronounced wind speed reduction. Such a feature is also observed at the 240 m leg (Figs. 14b, 15b) although to a lesser extent. It is also evident that the
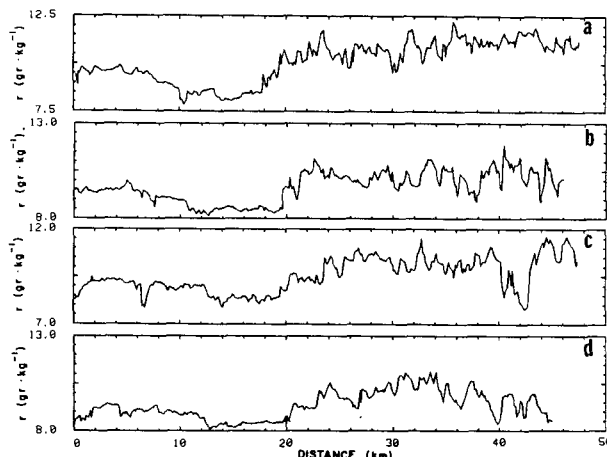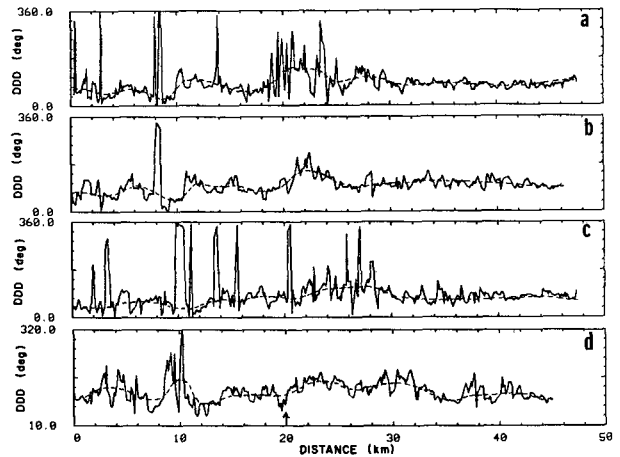
location of the coupling of both flows progressed with height towards the irrigated area, with the intensity of the thermal flow reducing with height.

On 28 July, three radiosonde measurements were carried out at the locations C1, in the irrigated area (altitude 1448 m AMSL; release at 1313 MDT); C2 at the boundary of the irrigated area–dry land region (altitude 1458 m AMSL; release at 1318 MDT); and at C3, several km away from the irrigated areas (altitude 1550 m AMSL; release at 1321 MDT) (see Fig. 1 for sites location). The profiles obtained are shown in Fig. 16 indicating the following specific features: (i) The depth of the PBL is shallowest over the irrigated area (C1), while the potential temperature within the PBL is noticeably higher at the dry land site (C3) as compared to that at C1 (by about 2 K). (ii) Deep over the irrigated area (C1), the moisture mixing ratio is higher within the PBL as compared to the other sites. The

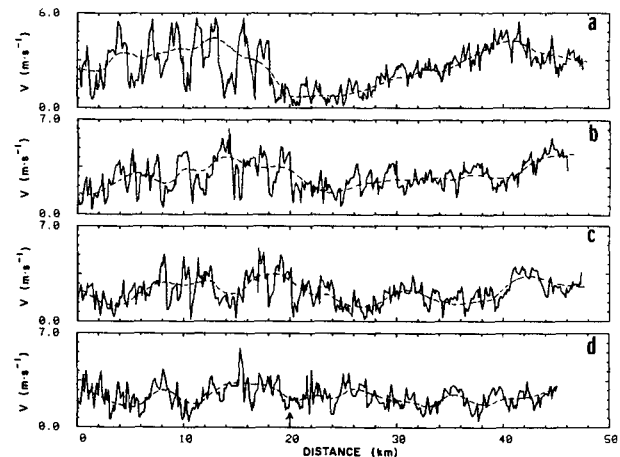FIG. 13. As in Fig. 12, except for moisture mixing ratio.

FIG. 15. As in Fig. 12, except for wind speed (the dashed line indicates a subjective estimate of the running mean).
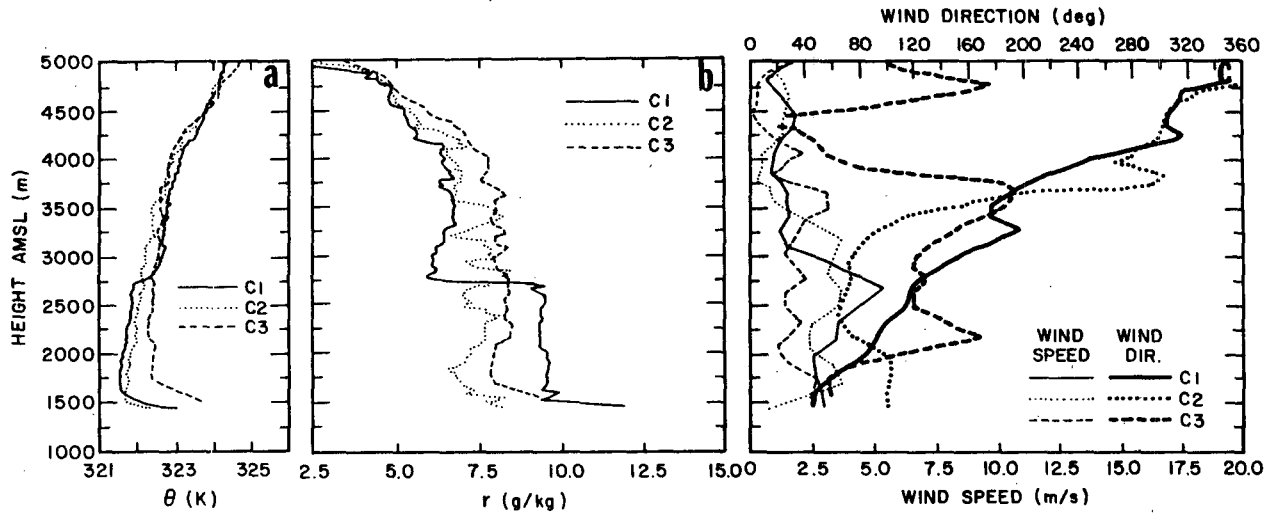
FIG. 16. Radiosonde measurements of (a) potential temperature, (b) moisture mixing ratio, and (c) wind at sites C1, C2 and C3 (indicated on Fig. 1) during flight 28.

high mixing ratio at this site is attributed to enhanced evapotranspiration, while vertical mixing of moisture is limited by the shallow boundary layer. (iii) Examination of the wind velocity profiles within the first 2000 m AGL indicates that the largest wind direction difference is about 90° whereas the corresponding wind speed difference reaches 2 m s^{-1}. In the first 500 m AGL profiles, C1 and C3 are quite similar with noticeable differences from that at C2.

d. Scaling considerations

A simplified scale analysis is performed in order to aid the interpretation of the observed features presented in the previous subsections.

1) NCMC CIRCULATION INTENSITY

Adopting the hydrostatic relation, the surface pressure difference, Δp_0, between a point in the middle of the irrigated domain and one in the dryland is given by

$$\Delta p_0 = p_z \left[\exp\left(\int_0^z \frac{g}{RT_i} \, dz \right) - \exp\left(\int_0^z \frac{g}{RT_{dl}} \, dz \right) \right] \quad (1)$$

where

p_z [≈ 800 mb] is assumed to be the pressure at level z over the measurements' area

z the height above the surface at which only a minor temperature difference between the dry land and the irrigated area is observed

g gravitational acceleration

T_i, T_{dl} temperatures above the irrigated and dry land, respectively ($\Delta T = T_{dl} - T_i$).

Flight and radiosonde results suggest for conservative

evaluations that no significant ΔT exists above $z \approx 600$ m (in flight 28 this height is somewhat higher); thus, using typical values, $\Delta T_{z=0} \approx 4$ K; and $\Delta T_{z=600} \approx 0$ yields for the dry atmosphere, $\Delta p_0 \approx 0.4$ mb. Assuming a typical variation of the mixing ratio of ≈ 5 g kg^{-1} between the dry land and the irrigated area, then the virtual temperature correction leads to $\Delta T_{v_{z=0}} \approx 3$ K, and a corresponding reduction of the pressure difference to $\Delta p_0 \approx 0.3$ mb. On the other hand, the supply of moisture into the atmosphere due to evapotranspiration over the irrigated area, results in an increase of atmospheric mass there and consequently a corresponding increase in the pressure. For example, an evapotranspiration amount of 0.1 cm of water into the atmosphere, results in a surface pressure increase of 0.1 mb when advection is negligible. Thus, overall it is suggested that $\Delta p_0 \approx 0.3$ to 0.4 mb. Table 1 summarizes data on horizontal temperature gradients obtained in observational studies and model simulations of sea-breeze flows. These results present selected values of ΔT and Δp_0 across a 20 km line centered (a) on the coastline, and (b) at the sea-breeze front. Selected observations and model results suggest ΔT at several hundred meters may reach 3 K across the coastline and across the sea-breeze front deep inland. It is suggested that the temperature changes observed along some of the transects in the current study are compatible to those indicated in some of the sea-breeze cases. Similar conclusions are suggested when considering Δp_0.

2) AVERAGED VERTICAL VELOCITY ALONG THE TRANSECT THROUGH THE SURFACE DISCONTINUITY

The flight results indicated a change of wind speed and direction as the transects cross between the irrigated

TABLE 1. Comparison of potential temperature gradients and surface pressure gradients obtained for sea-breeze circulations in various modeling and observational studies. (a) Observations of the temperature difference (ΔT) and surface pressure difference (Δp_0) along a 20 km line centered on, and normal to, the coastline during daytime under conditions favorable for sea breezes. Here, z_1, is near-surface height, $z_2 = 150$ m and $z_3 = 440$ m; G is the synoptic wind. (b) As in (a) except for a 20 km line across the sea-breeze front inland from the coastline. Source references as follows: [1]Lyons (1975); [2]Johnson and O'Brien (1973); [3]Hsu (1970); [4]Moroz (1967); [5]Clarke (1961); [6]Simpson et al. (1977); [7]Fisher (1961); [8]Neumann and Mahrer (1975); [9]Anthes (1978); [10]Physick (1976); and [11]Garratt and Physick (1985).

Reference	Date	Location	ΔT (K)			Δp_0 (mb)	G (m s^{-1})
			z_1	z_2	z_3		
(a)		*Observations*					
1	Aug 1971 (1400 local)	Lake Michigan	4.5	3.0	1.5	—	Light, onshore
2	Aug 1972 (1700 local)	Oregon Coast	7.0	—	—	—	—
3	June 1967 (1500 local)	Texas Coast	2.5	—	—	—	5 m s^{-1}, onshore
4	July 1964 (1600 local)	Lake Michigan	—	3.0	0.5	—	Light, parallel
5	Jan 1959 (1500 local)	S. Australia Coast	0.9	—	—	0.5	—
6	June 1973 (1700 local)	South Coast, UK	2.5	—	—	—	Light, onshore
		Model					
7	(1400 local)		≈5.0	≈4.0	≈1.0	—	Light
8	(1300 local)		6.5	2.0	<0.5	0.2	Light
9	(1600 local)		6.0	≈1.0	<0.5	0.25	Light
	$t \approx 6$ h		≈1.5	≈1.5	—	zero	
10	(1700 local) (run 4)		≈5.0	≈0.5	≈0.0	<0.3	Light
(b)		*Observations*					
5	27 Jan 1959 (1500 local) (1800 local)	Inland from Tailem Bend, S. Australia	1.1 0.9	— —	— −0.25	.08 —	—
5	22 Jan 1959 (2200 local)	Renmark, S. Australia	0.6	0.6	0.9	—	—
11	July–Aug 1974 (2300 local)	Far inland from coast in Northern Australia	≈0	≈4.0	≈2.0	0.5–1.0	6–12 m s^{-1}, onshore
		Model					
6	June 1973 (1000–1800 local)	Inland from South Coast, UK	0.3–2.5	—	—	—	Light, onshore
11	(2200 local)		≈0	≈2.5	≈2.0	0.3–0.8	6–12 m s^{-1}, onshore

and the dry land areas. As evident from the analysis in section 4a, the related thermal change should drive a thermally induced flow which is coupled with the background flow. The vertical velocity, $\bar{w}(z)$, at height z can be approximated by

$$\bar{w}(z) = -\int_0^z \left(\frac{\partial \bar{u}}{\partial x} + \frac{\partial \bar{v}}{\partial y}\right) dz \qquad (2)$$

where $\bar{u}$, $\bar{v}$ are the wind components along and normal to the flight transects, respectively. Since the flight transect is roughly normal to the surface discontinuity, $\partial \bar{u}/\partial x$ is the dominant component in Eq. (2) while considering the impact of NCMC on the flow.

Therefore, for a simplified scaling purpose, we can write Eq. (2) as

$$\bar{w}(z) \approx -\int_0^z \left(\frac{\partial \bar{u}}{\partial x}\right) dz. \qquad (3)$$

Table 2 summarizes $\bar{w}(z)$ values based on the flight data. In flight 28 in which the most noticeable NCMC features were observed, the largest vertical velocities were induced. At a height of about 450 m where temperature and wind contrasts are small, the implied $\bar{w}$ is ≈ 15 cm s^{-1} on a horizontal scale of 5 km. This value is about the same as the $\bar{w}$ maxima found in sea breezes *at this horizontal scale* (e.g., Physick 1976). The magnitude of vertical velocity is likely to be greater

TABLE 2. The vertical velocity induced along the irrigated area–dry land boundary as derived by Eq. (3). Here $\Delta \bar{u}$ is the wind speed change along the contrast line, Δx the distance involved with the wind change, Δz the depth of the appropriate layer, $\Delta \bar{w}(z)$ the contribution of the related layer to the vertical velocity, and $\bar{w}_{top}$ is the evaluated velocity at the top aircraft leg.

Flight no.	Leg height (m)	$\Delta \bar{u}/\Delta x/\Delta z$ m s^{-1}/km/m	$\Delta \bar{w}(z)$ cm s^{-1}
16(1)	180	1.25/10/180	1.1
16(2)	180	0.9/10/180	~0
25	160	1.8/10/160	0.8
25	250	1.8/10/90	0.2
25	350	1.2/10/100	0.0
25	445	0.6/10/95	0.7
			$\bar{w}_{top}$ = 1.7
28	140	3.0/5/140	6.3
28	240	0.9/5/100	3.9
28	345	0.9/5/105	2.7
28	440	0.5/5/95	1.8
			$\bar{w}_{top}$ = 14.7

at smaller horizontal scales, as is typically found in the sea-breeze case.

e. Equivalent potential temperature

In all the flights the observed equivalent potential temperature, θ_e, is noticeably higher over the irrigated section of the transect as compared to that over the dryland (Table 3), reflecting the large moisture differences between both areas. The observed high θ_e values over the irrigated area are confined to a relatively shallow PBL, capped by a temperature inversion. Conceptual evaluations by Carlson and Ludlam (1968), and following studies by Ogura et al. (1982), Colby (1984), Lakhtakia and Warner (1987) and Lannici et al. (1987), suggested that once this potentially higher energy air is tapped (most likely in our case by advection of convective cloud activity during the afternoon into the area, or the development of cumulus clouds in situ) it will mix with the lower θ_e air just above it to enhance the moist convective activity. It is suggested that a sud-

den enhancement of convective clouds advected into this area during summer afternoon is likely to occur.

Possible mechanisms for an increase in potential instability in the lower atmosphere beyond the irrigated area boundaries, and, hence, possible enhancement of moist convective activity there under supportive synoptic conditions, may be involved in the present study with (i) an increase in θ_e within the boundary layer over the eastern slopes of the Rocky Mountains through horizontal advection by upslope flows. The formation of convective clouds related to daytime induced upslope flows is a common summertime feature in this location (e.g., Klitch et al. 1985); and (ii) advection of high θ_e to the dry land area surrounding the irrigated area where a deeper convective PBL and possible NCMC-induced vertical velocities exist (see studies cited in section 1).

Finally, Fig. 17 provides a composite of visible satellite imagery at 1500 MDT during August 1986. It is evident that the irrigated area along the south Platte river does not, on average, develop convective cloudiness by that time of the day regardless of relatively high moisture found in the PBL. This is likely, due to subsidence along the south Platte River valley associated with the valley circulations. This subsidence must exert a significant influence by that time, preventing the release of the potential convective energy. Also, over the relatively flat terrain of the Yuma–Wray area (and eastward toward Kansas), relatively clear skies are indicated over the irrigated area. The area is surrounded by convective cloudiness. The last feature may imply suppression of convection over the irrigated area due to (i) reduction in sensible heat fluxes, and consequently reducing the convective cloud formation there (see e.g., Colby 1984) and/or (ii) suppression of the convective activity over the irrigated area as related to the NCMC induced subsidence motion.

TABLE 3. Typical equivalent potential temperature, θ_e, (K) over the irrigated and the dryland areas during the various aircraft measurements.

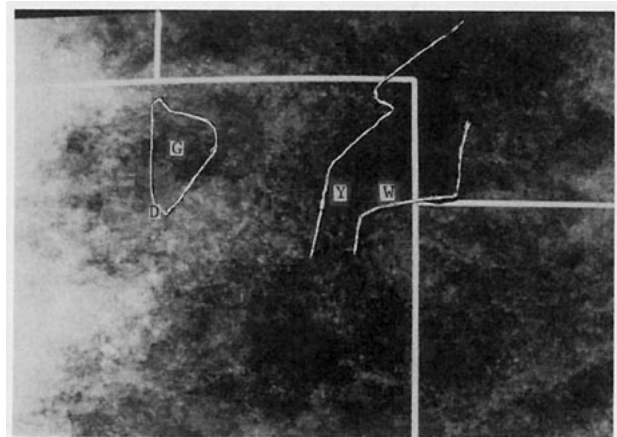| Flight	Height (m)	Irrigated area	Dry land
16(1)	130	350	342
16(2)	130	352	340
25	160	349	339
25	250	343	339
25	350	343	338
25	445	342	337
28	140	357	348
28	240	354	348
28	345	353	348
28	440	353	348

FIG. 17. Computer-averaged, visible wavelength satellite imagery for 1500 MDT August 1986. The estimated boundaries of the irrigated areas are marked by white lines. (D: Denver; G: Greeley; W: Wray; Y: Yuma).

5. Numerical model simulations

a. Modeling aspects

In order to provide additional interpretation to the observed mesoscale features presented in the previous sections, numerical model simulations were carried out for the area under study (see Fig. 1 for the simulated domain). The numerical model formulation is given in Pielke (1974), Mahrer and Pielke (1977), and McNider and Pielke (1981), and will not be repeated here. Previous simulations with this model applied to northeast Colorado (Abbs and Pielke 1986) indicate its capability to resolve the general summer mesoscale flows over the area.

In order to force the model as realistically as possible while considering the variability of land use over the studied area, we replaced the model-derived surface temperatures (which rely on the solution of the surface heat balance equation) by satellite-based estimates of surface temperatures. Adopting this approach, we avoid the need to specify vegetation and soil characteristics, and their related parameters, at the model grid points. On the other hand, since the surface evapotranspiration is not computed, corrections for virtual temperatures are not included in the model computations. Unfortunately, since there were inadequate GOES-derived IR blackbody surface temperature data available for the flight days, alternative simulations were considered. The IR GOES blackbody surface temperature composite based on the second half of July 1986, as indicated in section 3, was used for the surface thermal forcing of the model.

The simulations commenced at 0600 MDT when the surface temperature and air temperature are nearly equal. Hourly GOES IR surface temperature estimates were available for most of the simulation period. Missing surface temperature data were computed by interpolation; it was assumed there was a sinusoidal change in the IR surface temperature between 0600 and 1300 MDT. Similarly, surface temperatures were interpolated for intermediate numerical model time steps based on the two closest hourly surface temperature datasets. The composites tend to emphasize clear weather situations associated with high pressure systems since this was the dominant weather pattern during the last half of July 1986. Three illustrative simulations, assuming an initial potential temperature lapse rate of 3.5 K km^{-1}, were performed with (i) a zero mean synoptic flow; (ii) a southerly synoptic flow of 2.5 m s^{-1} (reflecting similar synoptic flow conditions to those of flight 16); and (iii) a northeasterly synoptic flow of 2.5 m s^{-1} (reflecting similar synoptic flow conditions to those of flight 28). The model grid points are 59 × 34, (the simulated domain is illustrated in Fig. 1) with $\Delta x = 6.9$ km. In the vertical, 20 levels were used with the model top at a height of 15 km. It should be noted that when the values of sensible heat

fluxes exceeded 500 W m^{-2} they were constrained to this value. Such situations occurred at a few grid points mostly along the Rocky Mountain section of the domain, where Sheaffer and Reiter (1987) evaluated the peak sensible heat fluxes during July to be around 500 W m^{-2}.

The specific objectives of the simulations are primarily to evaluate the impact of the irrigated areas on both the generation of NCMCs and on their modification of the background flow. The numerical simulations are designed to provide a further evaluation relating to this aspect by presenting the horizontal fields of (i) sensible heat flux and (ii) surface flow. The intensity of horizontal gradients in the sensible heat flux fields provide a quantification of the intensity of potential NCMCs (e.g., see the evaluations in Segal et al. 1988). Simulations with various background flow intensity and direction, on the other hand, should provide some insight into the potential distortion of the NCMC flow by larger-scale winds.

b. Simulation results

Selected fields for the three cases (at 1400 MDT) are presented in Figs. 18 and 19, including the surface sensible heat flux, the surface horizontal wind velocity field, and a west–east vertical cross section of the horizontal wind velocity in the middle of the domain. In the absence of synoptic flow, the sensible heat fluxes and wind speeds over the irrigated areas are noticeably less than those of adjacent dry land areas (see Fig. 1 and Fig. 18a). Along flight transect No. 1, sensible heat fluxes below 200 W m^{-2} are found over the irrigated area. These values are higher than the corresponding values over a water surface for typical sea-breeze cases (e.g., see Kondo 1975). On the other hand, over the dry land, the sensible heat fluxes reached values above 400 W m^{-2}. Segal et al. (1988) deduced that such variations in the sensible heat flux should force a noticeable NCMC. The thermally induced upslope flows are evident, as is the modification of these flows over and near the irrigated area due to the thermal gradient there, reflecting an NCMC influence in that region (Fig. 18b). Coincident with the irrigated area–dryland area contrast between Greeley (GR) and Briggsdale (BR), the flow tends toward the south with a light westerly component. In the Yuma area, an intensification of the surface flow, which appears to be related to a NCMC, is noticeable around the irrigated area. The features of the flow within the boundary layer are presented in Fig. 18c. The perturbation in the wind velocity in the Greeley area is noticeable within a depth of several hundred meters.

The second numerical simulation is the same as the previous one except for introducing a southerly synoptic flow of 2.5 m s^{-1} (Fig. 19a–c), analogous to that prevailing during flight 16. Stronger simulated flow caused somewhat higher sensible heat fluxes (Fig. 18a)
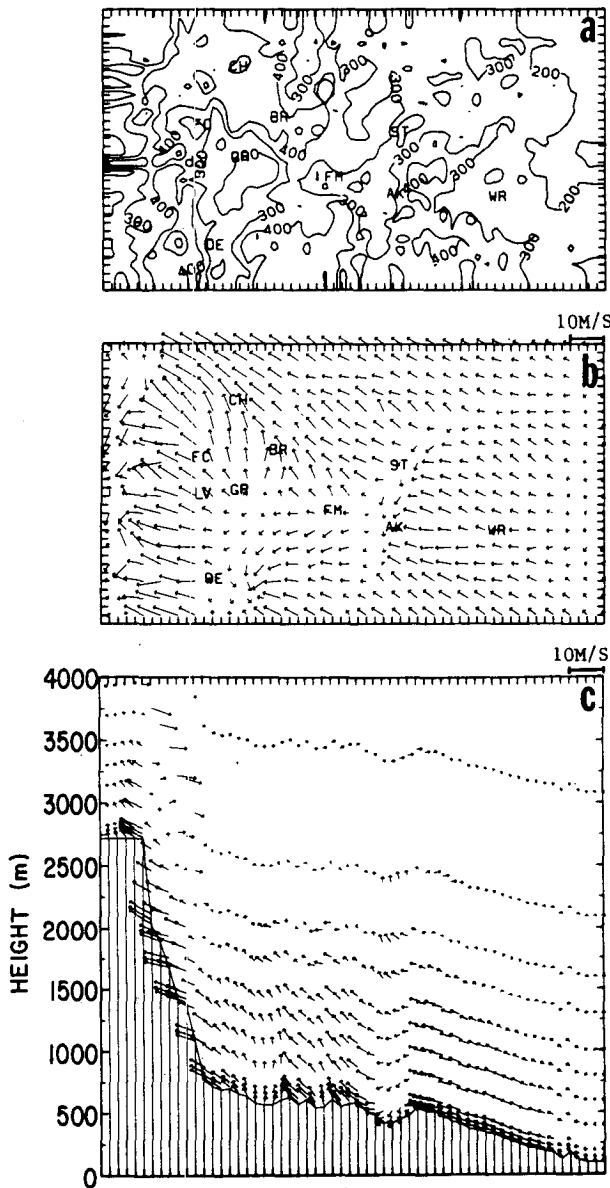
FIG. 18. Numerical model simulated fields at 1400 MDT for no-synoptic-flow case: (a) surface sensible heat fluxes (W m^{-2}); (b) surface horizontal wind velocity (at 5 m height); (c) east–west vertical cross section at the middle of the domain presenting the horizontal wind velocity; upward velocity vector indicates southerly flow (see Fig. 1 for the arrow indication of the cross-section location).

as compared to the previous case. However, the correspondence of comparatively low sensible heat flux values over the irrigated areas is pronounced, as in the previous case. The general intensification of the initial flow in the simulated domain due to dynamical effects and thermally induced upslope circulations is quite apparent, reducing somewhat the impact of the thermally induced flows involved with the irrigated areas of Greeley and Yuma (Fig. 19b). The east–west vertical cross section, presenting the wind velocity field at the

middle of the simulated domain, shows a strong south-easterly flow in the lower atmosphere, perturbed somewhat within a shallow layer over the irrigated area of Greeley (Fig. 19c).

When a NE synoptic flow of 2.5 m s^{-1} is introduced in the third simulation, analogous to that found in flight 28, the previous characteristics of sensible heat flux are retained (Fig. 19d). The impact of the irrigated area through thermal-induced flow on the local wind field is more noticeable as compared to the previous case (Fig. 19e, f).

In conclusion, the simulation results presented in this paper indicate that the thermally induced flow related to the irrigated areas was most pronounced for the zero mean synoptic flow and to some extent for the NE flow cases. For these cases the impact upon the flow was noticeable up to several hundred meters above ground. The computed differences in the surface sensible heat fluxes between the irrigated areas and the adjacent dry land were considerable; however, lower than those expected for an equivalent sea-breeze situation.

6. Summary and conclusions

The present study was designed to evaluate the nature of NCMCs associated with irrigated crop areas in northeast Colorado. Satellite IR imagery, surface and PBL measurements, as well as numerical model simulations, were adopted for this purpose. Satellite-derived estimates of surface temperatures correspond well with land use. Over the irrigated areas the IR surface temperatures were lower by about 10 K than those over the adjacent dry land. Aircraft and surface measurements indicated a noticeable drop of the air temperature and increase in moisture at low levels over the irrigated area as compared to the surrounding dry land. This difference was evident up to a height of about 445 m which was the aircraft's upper measurement level. The aircraft measured significant changes in the temperature, moisture, and flow fields. These changes are clearly related to the change in land use along the transects. Similarly, differences in the equivalent potential temperature were measured within the lower PBL. Radiosonde measurements in one of the cases suggested some suppression of the PBL depth over the irrigated areas.

No sharply defined NCMC flow was evident in the three observational case studies. It is suggested that the coupling of the NCMC flow with the existing thermally induced upslope flow in the area and the synoptic flow, prevented the clear recognition of the NCMC flow. The characteristics of the changes in the wind speed and direction along the flight transects as well as in the surface observations support this conclusion. It is worth noting that most large irrigated areas are within river basins. As such, they occur within valleys with various degrees of steepness. Consequently, the pure NCMC
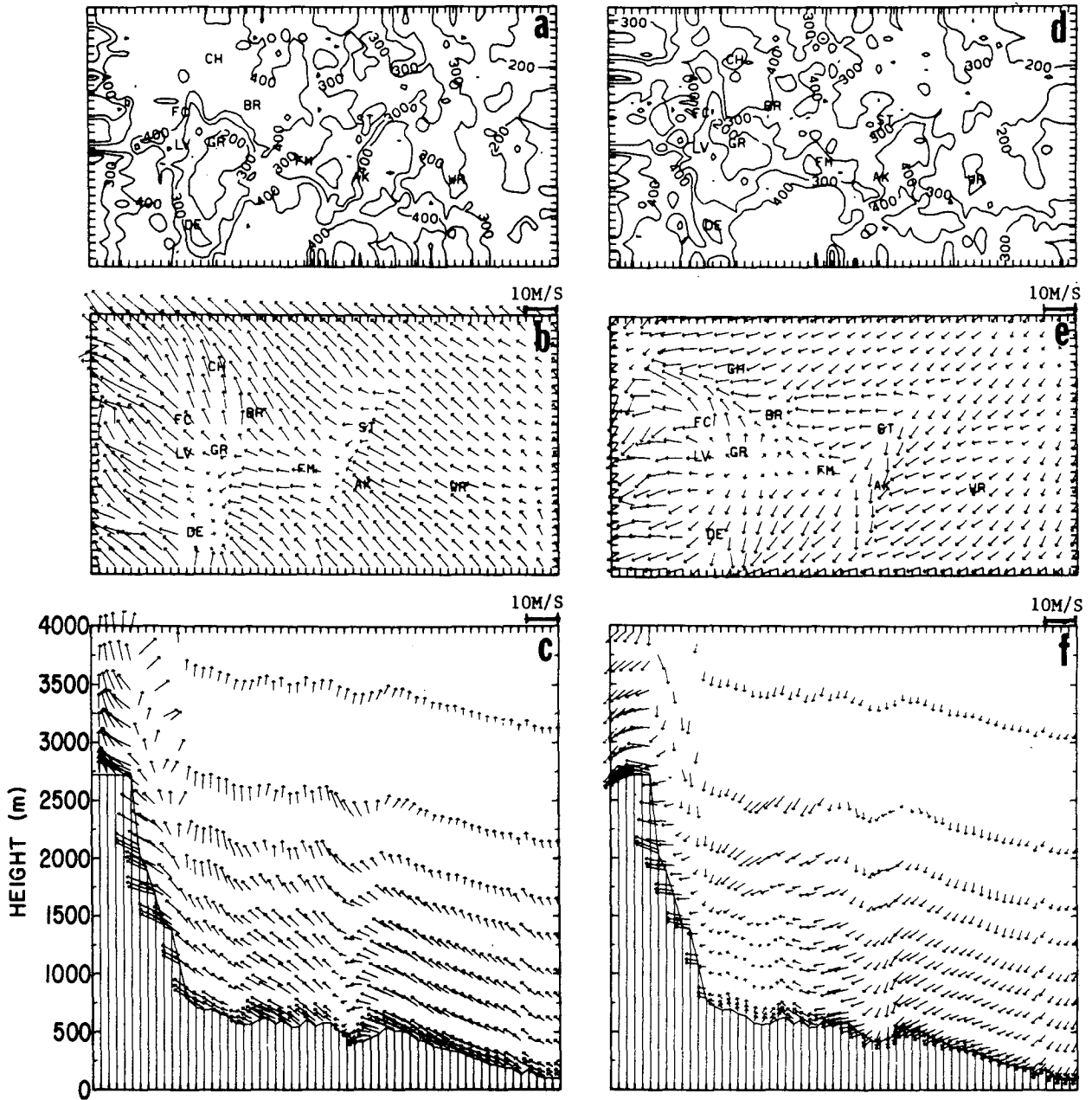
FIG. 19. As Fig. 18 except for (a–c) southerly synoptic flow of 2.5 m s^{-1}; and for (d–f) northeasterly synoptic flow of 2.5 m s^{-1}.

is likely to be difficult to resolve, since the flow field would also be affected by thermally induced upslope flows. However, some of the low-level, horizontal temperature gradients identified in this study (and the implied surface pressure gradient across the contrast line), were found to be comparable to typical values associated with moderate sea breezes, and therefore suggestive of the potential development of NCMCs. Numerical model simulations indicate that the thermally induced upslope flow in the area produces some masking of the NCMC flow pattern.

The suggestion that NCMCs over irrigated areas may be related to convective cloud formation requires observational evaluation of the following: (i) Is the development of thermal gradients in the PBL between large irrigated areas and adjacent dry land typically of sufficient intensity and spatial extent to generate significant NCMCs in *real world* situations (i.e., on same order as found for sea-breeze circulations)? It may be that most irrigated areas are not large enough in their horizontal scale (e.g., 20–30 km), or otherwise not sufficiently dense with crops at any given time; (ii) In

824   MONTHLY WEATHER REVIEW   VOLUME 117

areas for which (i) is positively confirmed, and for situations which have supportive synoptic conditions, study is required of the magnitude of flow and moisture convergence necessary to generate regions of deep cumulus convection. Further observations should be carried out in order to comprehensively evaluate to what extent the area studied in the present paper fulfills (i) and (ii).

Other promising areas in the United States which may be considered during the summer for such a purpose include, for example, the irrigated areas in the Columbia Plateau; Washington state (mostly in Franklin County and some irrigated areas along the Yakima River); Caldwell, Twin Falls, and the Idaho Falls areas along the Snake River in Idaho; the irrigated areas north of the Canadian River in the panhandle of Texas; the Rio Grande Valley area in south Texas; the irrigated areas in southwest and northwest Kansas; and the irrigated areas in southwest Nebraska. The irrigated areas in the Central Valley and south of the Salton Sea in California, and the southern surrounding area of Phoenix, Arizona provide examples for locations with potential for relatively intense NCMC, though (ii) above is not likely to be fulfilled.

y

REFERENCES

Abbs, D., and R. A. Pielke, 1986: Thermally forced surface flow and convergence patterns over northeast Colorado. *Mon. Wea. Rev.,* 114, 2281–2296.

Anthes, R. A., 1978: The height of the planetary boundary layer and the production of circulation in a sea-breeze model. *J. Atmos. Sci.,* 35, 1231–1239.

——, 1984: Enhancement of convective precipitation by mesoscale variations in vegetative covering in semiarid regions. *J. Climate Appl. Meteor.,* 23, 541–554.

Brown, E. N., C. A. Friehe and D. H. Lenschow, 1983: The use of pressure fluctuations on the nose of an aircraft for measuring air motion. *J. Climate Appl. Meteor.,* 22, 171–181.

Carlson, T. N., and F. H. Ludlam, 1968: Conditions for the occurrence of severe local storms. *Tellus,* 20, 203–226.

Clarke, R. H., 1961: Mesostructure of dry cold fronts over featureless terrain. *J. Meteor.,* 12, 715–735.

Colby, F., 1984: Convective inhibition of a predictor of convection during AVE-SESAME II. *Mon. Wea. Rev.,* 112, 2239–2252.

Dzerdeevskii, B. L., Ed., 1963: *Sukhoveis and Drought Control.* Israel Program of Scientific Translations, 344 pp.

Fisher, E. L., 1961: A theoretical study of the sea-breeze. *J. Meteor.,* 18, 216–233.

Garratt, J. R., 1987: The stably stratified internal boundary layer for steady and diurnally varying offshore flow. *Bound.-Layer Meteor.,* 38, 369–394.

——, and W. L. Physick, 1985: The inland boundary layer at low latitudes: II Sea-breeze influences. *Bound.-Layer Meteor.,* 33, 209–231.

——, and B. F. Ryan, 1988: The structure of the stably stratified internal boundary layer in offshore flow over the sea. *Bound.-Layer Meteor.* (in press).

Green, R. N., and M. Kruidenier, 1982: Interactive data procession of mesoscale forecasting applications. *Proc. Ninth Conf. on Weather Forecasting and Analysis.* Amer. Meteor. Soc., 60–64.

Hsu, S-A., 1970: Coastal air-circulation system: Observations and empirical model. *Mon. Wea. Rev.,* 98, 487–509.

Jarvis, P. G., and J. I. L. Morison, 1981: The control of transpiration and photosynthesis by stomata. *Stomatal Physiology,* Society for Experimental Biology, University of Cambridge, 248–279. [ISBN-0-521-23683-5.]

Johnson, A., and J. J. O'Brien, 1973: A study of an Oregon sea breeze event. *J. Appl. Meteor.,* 12, 1267–1283.

Klitch, M. A., J. F. Weaver, F. P. Kelly and T. H. Vonder Haar, 1985: Convective cloud climatologies constructed from satellite imagery. *Mon. Wea. Rev.,* 113, 326–337.

Kondo, J., 1975: Air sea bulk transfer coefficients in diabatic conditions. *Bound.-Layer Meteor.,* 9, 91–112.

Lakhtakia, M. N., and T. Warner, 1987: A real data study of the development of precipitation along the edge of elevated mixed layer. *Mon. Wea. Rev.,* 115, 156–168.

Lannici, J. M., T. N. Carlson and T. Warner, 1987: Sensitivity of the Great Plains severe-storm environment to soil-moisture distribution. *Mon. Wea. Rev.,* 115, 2660–2673.

Lee, R., 1978: *Forest Micrometeorology,* Columbia University Press, 276 pp.

Lyons, W. A., 1975: Turbulent diffusion and pollutant transport in shoreline environments. *Lectures on Air Pollution and Environmental Impact Analyses,* D. A. Haugen, Ed., Amer. Meteor. Soc., 136–208.

Mahfouf, J. F., E. Richard and P. Mascart, 1987: The influence of soil and vegetation on the development of mesoscale circulations. *J. Climate Appl. Meteor.,* 26, 1483–1495.

Mahrer, Y., and R. A. Pielke, 1977: A numerical study of the airflow over irregular terrain. *Contrib. Atmos. Phys.,* 50, 98–113.

——, and M. Segal, 1979: Simulation of advective Sharav conditions over Israel. *Israel J. Earth Sci.,* 28, 103–106.

McNider, R. T., and R. A. Pielke, 1981: Diurnal boundary layer development over sloping terrain. *J. Atmos. Sci.,* 38, 2198–2212.

Miller, E. R., and R. B. Friesen, 1985: Standard output data produces from the NCAR Research Aviation Facility. Bull. no. 9, Research Aviation Facility, NCAR, Boulder, CO, 9 pp.

Moroz, W. J., 1967: A lake breeze on the eastern shore of Lake Michigan: Observation and model. *J. Atmos. Sci.,* 24, 337–355.

Neumann, J., and Y. Mahrer, 1975: A theoretical study of the lake and land breezes of circular lakes. *Mon. Wea. Rev.,* 103, 474–485.

Ogura, Y., H.-M. Juang, H.-M. Zhang and S.-T. Soong, 1982: Possible

triggering mechanisms for severe storms in SESAME-AVE IV. *Bull. Amer. Meteor. Soc.,* **63,** 503–515.

Physick, W. L., 1976: A numerical model of the sea-breeze phenomenon over a lake or gulf. *J. Atmos. Sci.,* **33,** 2107–2135.

Pielke, R. A., 1974: A three-dimensional numerical model of the sea breeze over south Florida. *Mon. Wea. Rev.,* **102,** 115–139.

——, and M. Segal, 1986: Mesoscale circulations forced by differential terrain heating. *Mesoscale Meteorology and Forecasting,* P. Ray, Ed., Amer. Meteor. Soc., 516–548.

Segal, M., R. A. Pielke and Y. Mahrer, 1984: Evaluation of surface sensible heat flux effects on the generation and modification of mesoscale circulations. *Proc. Second Int. Symp. on Nowcasting,* European Space Agency, Norrkoping, Sweden, 263–269.

——, R. Avissar, M. C. McCumber and R. A. Pielke, 1988: Evaluations of vegetation effects on the generation and modification of mesoscale circulations. *J. Atmos. Sci.,* **45,** 2268–2292.

Sheaffer, J. D., and R. Reiter, 1987: Measurements of surface energy budgets in the Rocky mountains of Colorado. *J. Geophys. Res.,* **92,** 4145–4162.

Simpson, J. E., D. A. Mansfield and J. R. Milford, 1977: Inland penetration of sea-breeze fronts. *Quart. J. Roy. Meteor. Soc.,* **103,** 47–76.

Smith, B., and L. Mahrt, 1981: A study of boundary layer pressure adjustments. *J. Atmos. Sci.,* **18,** 334–346.

Smolarkiewicz, P. K., and T. L. Clark, 1985: Numerical simulation of the evaluation of a three-dimensional field of cumulus clouds. Part I: Model description, comparison with observations and sensitivity studies. *J. Atmos. Sci.,* **42,** 502–522.

Sun, W.-Y., and Y. Ogura, 1979: Boundary-layer forcing as a possible trigger to a squall line formation. *J. Atmos. Sci.,* **36,** 235–254.

Toth, J. J., and R. H. Johnson, 1985: Summer surface flow characteristics over northeast Colorado. *Mon. Wea. Rev.,* **113,** 1458–1469.

Yan, H., and R. A. Anthes, 1988: The effect of variations in surface moisture on mesoscale circulations. *Mon. Wea. Rev.,* **116,** 192–208.